CHALMERS
UNIVERSITY OF TECHNOLOGY

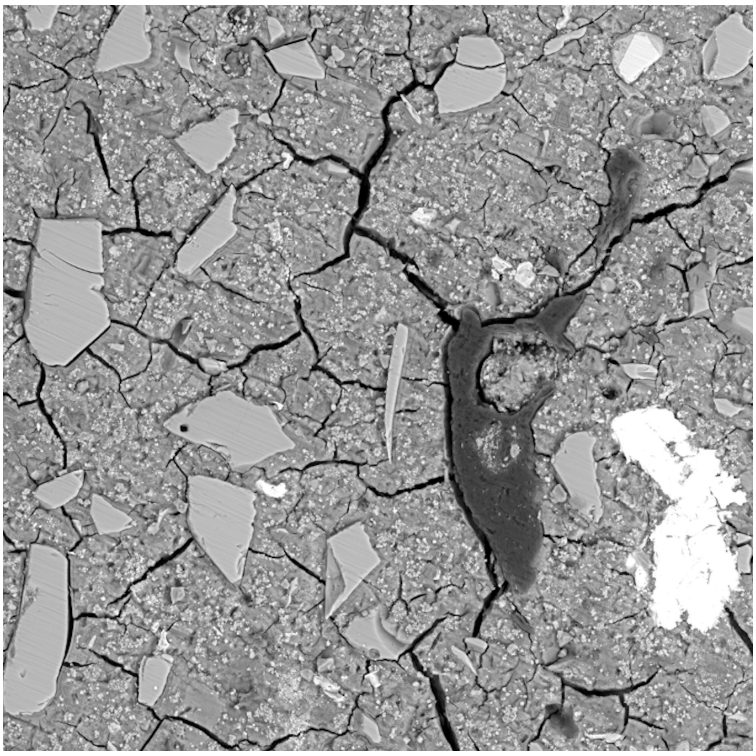

Potential of carbonated industrial by-products in the synthesis of green construction materials

Master's thesis in Materials Chemistry

HANNAH SVANBERG

DEPARTMENT OF CHEMISTRY AND CHEMICAL ENGINEERING

CHALMERS UNIVERSITY OF TECHNOLOGY
Gothenburg, Sweden 2026
www.chalmers.se

Master's thesis 2026

Potential of carbonated industrial by-products in the synthesis of green construction materials

HANNAH SVANBERG

CHALMERS
UNIVERSITY OF TECHNOLOGY

Department of Chemistry and Chemical Engineering
Division of Applied Chemistry
Chalmers University of Technology
Gothenburg, Sweden 2026

Potential of carbonated industrial by-products in the synthesis of green construction materials
HANNAH SVANBERG

Supervisors: Jenny Bengtsson & Emmanouela Leventaki, Applied Chemistry
Examiner: Diana Bernin, Applied Chemistry

Master's Thesis 2026
Department of Chemistry and Chemical Engineering
Division of Applied Chemistry
Chalmers University of Technology
SE-412 96 Gothenburg
Telephone +46 31 772 1000

Cover: SEM image of alkali-activated material using 40 wt% CPT

Typeset in LaTeX
Printed by Chalmers Reproservice
Gothenburg, Sweden 2026

Potential of carbonated industrial by-products in the synthesis of green construction materials

HANNAH SVANBERG
Department of Chemistry and Chemical Engineering
Chalmers University of Technology

Abstract

Carbonated steel slags have been proposed as a potential precursor in alkali-activated materials, due to their ability to both utilize industrial by-products and store CO_2. However, the influence of carbonation on the reactivity and performance of steel slags in alkali-activated systems remains largely unexplored. This thesis investigates the use of carbonated Petrit T (CPT), a by-product from sponge iron production, as a co-binder in alkali-activated materials.

Blast furnace slag was used as the primary binder, and was replaced with different mass ratios of CPT. The resulting materials were evaluated with respect to reaction kinetics, phase formation, porosity, microstructure and mechanical performance. The materials were evaluated in terms of setting time, heat evolution during reaction, phase development, molecular structure, surface area, microstructure, elemental composition and compressive strength.

The results showed that CPT influenced the reaction behavior of the systems. Low CPT content accelerated the initial setting behavior, while higher replacement levels delayed later reaction stages and reduced mechanical performance. TGA and FTIR analyses confirmed the formation of C–A–S–H gel phases in all alkali-activated samples. They also showed that the carbonate related phases were present after alkali activation and increased with increasing CPT content. BET analysis showed that pore volume and specific surface area increased with increasing CPT content, indicating the formation of a more porous microstructure. SEM/EDS observations revealed the presence of unreacted BFS and CPT particles, suggesting limited participation in gel formation.

Overall, the results indicate that carbonated steel slags can be incorporated into AAMs and contribute to CO_2 storage through mineral carbonation. However, at the investigated replacement levels, CPT behaved more as an inert filler and negatively impacted the mechanical performance of the materials.

Keywords: Alkali-activated materials; Carbonated steel slag; Mineral carbonation; Industrial by-products; C–A–S–H; Sustainable binders; CO_2 sequestration

Acknowledgements

I would like to express my sincere gratitude to my supervisors, Emmanouela Leventaki and Jenny Bengtsson, for their guidance, support and valuable feedback throughout this thesis project. Their expertise and encouragement have been invaluable during both the experimental work and the writing process. I would also like to thank Helén Jansson for her assistance in the ACE Laboratory and for her help with the practical aspects of the experimental work. Furthermore, I would like to thank my examiner, Diana Bernin, for creating a welcoming and positive research environment and for making us master's students feel included in the research group. Finally, I would like to thank my family and friends for their continuous support and encouragement during my studies.

Hannah Svanberg, Gothenburg, May 2026

List of Abbreviations

Below is the list of abbreviations that have been used throughout this thesis listed in alphabetical order:

AAM	Alkali-Activated Material
BFS	Blast Furnace Slag
C–A–S–H gel	Calcium-Alumino-Silicate-Hydrate gel
CPT	Carbonated Petrit T

Contents

List of Figures

List of Tables

1
Introduction

Cement and the concrete industry represent some of the most essential construction materials globally, resulting in extensive consumption and making them a major contributor to CO_2-gas emissions [1]. The emissions originate from the combustion of fossil fuels, electricity generation and process-related chemical reactions, particularly the calcination of limestone [2]. In addition to the environmental impact, cement production is highly energy-intensive, further emphasizing the need for alternative binder systems with lower carbon footprints.

A promising alternative to ordinary Portland cement as a binder is the use of by-products from the iron and steel industry, such as blast furnace slag (BFS) and other steel slag. BFS is already used to some extent as a partial cement replacement and has been shown to enhance long-term strength development, although it typically results in lower early-age strength. In contrast, steel slags are utilized to a much lesser extent, primarily due to their volume instability and low hydraulic reactivity [3]. These limitations have restricted their broader application in construction materials despite their large availability.

Alkali-activated materials (AAM) provide a pathway to utilize these industrial by-products. These precursors require activation with an alkaline solution, preferably a combination of sodium silicate and sodium hydroxide, to dissolve the solids and enable the formation of a binding network [4]. Depending on the precursor composition, particularly the calcium content, it leads to formation of networks such as calcium aluminosilicate hydrate (C–A–S–H) gel phases and thus affect the microstructure and mechanical properties of the material.

To overcome the limitations of steel slag, carbonation has been proposed as an approach. During carbonation, alkaline components in the slag react with CO_2 to form stable carbonate phases, primarily $CaCO_3$. This process enables CO_2 capture and storage while also enhancing the chemical stability of the slag [5]. However, while carbonation enhances stability, it may simultaneously reduce the availability of reactive calcium species required for gel formation in the AAM. This creates a potential trade-off between stability and reactivity, which may affect the performance of the resulting material.

Despite increasing interest in carbonated steel slag, its behavior in alkali-activated systems remains insufficiently understood. In particular, the extent to which carbonated steel slag participates in binder formation, as opposed to acting as an inert

filler, is unclear. Furthermore, its effects on reaction kinetics, microstructure development, porosity and mechanical performance have not been fully established.

1.1 Aim

The aim of this thesis is to evaluate the use of a carbonated steel slag as a co-binder in alkali-activated materials. Different mass ratios of carbonated Petrit T, a by-product from the manufacture of sponge iron, are investigated. The effects on material properties, including mechanical performance, porosity and microstructure, are assessed.

1.2 Specification of the issue investigated

- How does CPT affect reaction kinetics and setting behavior?
- How does CPT influence pore structure and surface area?
- Does CPT contribute to or hinder strength development?
- Does CPT act as a reactive binder or inert filler?

1.3 Limitations

The work is limited to laboratory scale and will not address the full-scale production or long-term durability of the AAM. The modulus of the alkali-activator will not be varied and one type of carbonated steel slag will be tested.

2
Theory

The following sections provide the theoretical background relevant to this study, including ordinary Portland cement, alkali-activated materials and carbonated steel slags.

2.1 Ordinary Portland cement

Cement is a hydraulic binder that forms a plastic paste when mixed with water, that gradually hardens into a solid material and is capable of binding aggregates together. The hardening process can occur in both air and water and the material continues to gain strength over time. Ordinary Portland cement (OPC), the main binder used in concrete, consists primarily of Portland cement clinker together with 0–5% limestone or blast furnace slag [6].

Portland cement clinker is produced by grinding and mixing limestone, clay and iron ore, then sintered in a rotary kiln at temperatures up to approximately 1450°C [7] [6]. The resulting clinker mainly contains calcium silicates and calcium aluminates, together with smaller amounts of free calcium oxide, magnesium oxide and alkali elements [6].

When OPC is mixed with water, hydration reactions that primarily leads to the formation of calcium silicate hydrate (C–S–H) occurs, which is the main strength-giving network. During curing, the cement mixture develops a heterogeneous microstructure consisting of crystalline phases, gel phases, unreacted particles, pore structures and water [6].

2.1.1 Environmental impact of OPC

Despite its widespread use, OPC production is associated with large environmental impacts. The manufacturing of cement accounts for approximately 7% of global CO_2 emission, and each tonne of cement produces around 0.7–1.9 tonne of CO_2 [8]. A major source of the emissions comes from the calcination of limestone in the clinker production, where approximately 0.5 tonnes of CO_2 are released for every tonne of clinker [7]. Additionally, cement production is highly energy-intensive, where energy consumption accounts for roughly 50–60% of the total production cost [8].

Portland cement remains the dominant construction binder due to the large avail-

ability of limestone, the reliability of the existing production and more than 150 years of implementation and standardization. Existing construction standards are largely based on the use of OPC systems, which contributes to its widespread use [7].

2.2 Alkali-activated materials

In alkali-activated materials, a highly alkaline solution depolymerizes the aluminosilicate precursor into reactive silicate and aluminate species. Common activators are alkali hydroxides, alkali silicates, alkali carbonates or combinations of them [7]. During the reaction process, dissolution of the precursor is followed by condensation and hydration reactions, that form binding gel phases. The type of gel network formed depends on the calcium content and alkalinity of the system [4, 9].

Blast furnace slag (BFS) and steel slag are calcium-rich precursors, which means that their reaction mechanism differs from low-calcium geopolymeric systems. Calcium-rich AAMs mainly generate calcium aluminosilicate hydrate (C–A–S–H) gels, which are structurally similar to the C–S–H gels found in ordinary Portland cement [4, 10]. In C–A–S–H gels, aluminum partially substitutes silicon in the tetrahedral structure. This results in longer silicate chains, higher degree of polymerization and increased crosslinking, compared to conventional C–S–H gels [10]. The C–A–S–H structure can contain up to 13 tetrahedra, while C–S–H gels typically contain only three to five. Additionally, C–A–S–H gels have a higher proportion of Q^3 species, indicating a more crosslinked structure [10]. Here, Q^1 refers to an end-of-chain Si or Al tetrahedron, Q^2 to a mid-chain tetrahedron and Q^3 to a cross-linking tetrahedron [7, 11].

During hydration, the solid precursor dissolves into reactive monomers such as $Si(OH)_4$, $[SiO_2(OH)_2]^{2-}$, $[SiO(OH)_3]^-$, $[Al(OH)_4]^-$, and free Ca^{2+} ions. These species recombine and precipitate as C–A–S–H gel phases [12]. Depending on the composition of the precursor and on the activator type, secondary phases such as hydrotalcite or zeolites may form, particularly at higher aluminum contents [4]. In some systems, sodium aluminosilicate hydrate (N–A–S–H) might coexist with C–A–S–H gels, especially when using silicate-based activators. These sodium-rich phases generally have lower degrees of crystallinity [4, 7].

2.2.1 Alkali-activators

Hydroxides, silicates or a combination of both are often used as activators in AAM systems. Silicate activators contribute additional reactive silica, which dissolves and reacts faster than the silica present in the precursor. This generally improves the mechanical performance of the AAM [4]. Systems activated solely by hydroxides have higher pH but often produce weaker structures and entail environmental and personal safety risks due to their highly corrosive nature. Combined hydroxide-silicate activators are often preferred, as they promote stable reaction products and have relatively short curing times [4].

2.3 Steel slags as binders in alkali-activated materials

Steel slags are major by-products from the steel industry, and utilization of these materials is important both from environmental and resource-efficiency perspectives. There are two main routes to produce steel: the blast furnace-basic oxygen furnace route or the electric arc furnace route. The slags generated from these routes differs in composition and properties [13].

2.3.1 Blast furnace slag

Blast furnace slag (BFS) is mainly composed of calcium, silicon, aluminum and magnesium, and is widely used as a supplementary cementitious material (SCM) and precursor in alkali-activated materials.

2.3.2 Steelmaking slags

Steel slags from the electric arc furnace route differs from BFS in its composition, as it is richer in calcium, silicon, and iron, although exact composition differs depending on production process. These slags are less commonly used as SCM due to their poor volume stability and low hydraulic reactivity. The instability is mainly due to the presence of free CaO and MgO, which forms $Ca(OH)_2$ and $Mg(OH)_2$ upon contact with water. These hydration reactions lead to expansion, cracking and dimensional instability in the material [13]. In addition, some steel slags might contain heavy metals, which further complicates their utilization [13].

2.3.3 Carbonated steel slags

Carbonation have been proposed as a strategy to improve both performance and stability of steel slags in AAM systems. During carbonation, CO_2 reacts with alkaline components in the slag, primarily CaO, forming stable carbonate phases such as $CaCO_3$ [5, 14]. This provides a dual environmental benefit, as carbonation both enables CO_2 storing and improves the material properties of the slag [5]. Steel slags have a high carbonation potential and studies have shown that they can absorb large amounts of CO_2 while simultaneously increasing the chemical stability of the material through the formation of stable carbonates [14].

Carbonated slags have been suggested as a way to overcome the limitations with untreated steel slags in AAMs. Carbonation improves volume stability by reducing the amount of free CaO and suppressing hydration reactions [15]. Furthermore, the formed $CaCO_3$ particles can increase the specific surface area of the system and provide additional nucleation sites for reaction products, potentially acceleration early-age reactions [15]. However, carbonation may also reduce the dissolution of reactive Ca–Si–Al species from the precursor and lower the alkalinity of the mix. As a result, high replacement levels of carbonated slag can lead to reduced mechanical strength [15].

3
Materials and methods

The following sections describe the materials used in this project, including both the precursors and the activators. The sample preparation procedure and the characterization methods are also presented.

3.1 Raw Materials

The raw materials used for the preparation of the alkali activated materials are presented in this section. Their origin and composition are described in the following subsections.

3.1.1 Precursors

Two different slags were used as binders. Merit is a blast furnace by-product, primarily composed of Si, Ca, Al and Mg oxides. Petrit T is a by-product from sponge iron production and is consists mainly of Si, Ca and Al oxides, as well as carbon. The chemical composition of the two slags is presented in Table 3.1. Both materials are commercially available industrial by-products, with Merit supplied by Swecem and Petrit T by Höganäs.

Table 3.1: Chemical composition of Merit and Petrit T.

Compound	Merit (wt%)	Petrit T (wt%)
SiO_2	36	18
CaO	34	37
MgO	13	–
Al_2O_3	13	9
TiO_2	1.8	–
Na_2O_{eq}	1.0	–
K_2O	0.70	–
Na_2O	0.55	–
MnO	0.41	–
FeO	0.38	–
Fe_2O_3	–	7
C	–	20

The steel slag used in this study, Petrit T, was carbonated prior to this work as

part of a separate investigation. The carbonation was performed through direct aqueous mineral carbonation, in which CO_2 reacts with the slag in a water-based system. During the process, metal ions present in the slag dissolve into the aqueous phase, while dissolved CO_2 forms reactive CO_3^{2-} and HCO_3^- species. These species subsequently react with the dissolved metal ions to form stable metal carbonates, primarily $CaCO_3$ [16]. The carbonated Petrit T (CPT) used in this study sequestered approximately 150 kg CO_2 per tonne of raw Petrit T. Non-carbonated Petrit T was also used to investigate the effect of carbonation on the performance of Petrit T as a binder in the AAM.

3.1.2 Activator

The alkali activator used in this study was a mixture of sodium silicate, sodium hydroxide and deionized water. The sodium silicate had a composition of 8 wt% SiO_2 and 27 wt% Na_2O, while the sodium hydroxide had a concentration of 50 wt%. The activator was prepared to have a Na/Si molar ratio of 1.0 and 30 wt% solid content. The combination of sodium silicate and sodium hydroxide provides both alkalinity and soluble silicate species that promotes the dissolution of the slag as well as the formation of C–A–S–H type gels.

3.2 Sample preparation

The activator was prepared in advance and added to the binder-mixture, keeping the water-to-binder ratio (L/S) fixed at 0.5 for all mixtures. Carbonated Petrit T (CPT), non-carbonated Petrit T (NCPT) and Merit was used as binders in different ratios, as shown in table 3.2. The mixtures were then manually stirred until a homogeneous mixture was achieved.

Table 3.2: Mix proportions of the investigated samples.

Sample	Merit (g)	CPT (g)	NCPT (g)	Alkali activator (g)
CPT 0% (ref)	50	0	0	31.3
CPT 10%	45	5	0	31.3
CPT 15%	42.5	7.5	0	31.3
CPT 20%	40	10	0	31.3
CPT 25%	37.5	12.5	0	31.3
CPT 30%	35	15	0	31.3
CPT 40%	30	20	0	31.3
NCPT 20%	40	0	10	31.3

3.3 Characterization methods

Several different characterization techniques were used to evaluate the carbonated binders influence on the AAMs properties. The analyses focused on reaction kinetics,

phase evolution, microstructure, porosity and mechanical strength, and is described in the following subsections. The recorded data were exported as text files and processed and plotted using Python.

3.3.1 Reaction kinetics and setting behavior

The initial setting time was determined using the Vicat test. Samples were prepared using 50 g binder and 31.3 g alkali-activator. A needle with a 300 g weight on top penetrated the sample at regular intervals of 5–10 minutes and the penetration depth was recorded for each measurement. As the material hardened, the penetration depth decreased gradually over time due to the formation of gel phases within the system. The recorded penetration depths were plotted as a function of time and the data were normalized to enable comparison between samples. The initial setting time was defined as the point at which the needle penetration corresponded to 80% of the sample height.

Isothermal calorimetry was used to measure the heat evolution during the hardening of the AAMs. For each composition (0% CPT, 20% CPT, 40% CPT and 20% NCPT), two replicate samples were prepared and transferred immediately after mixing into the calorimeter ampules. The measurements were conducted at a constant temperature of 20°C and the heat flow was recorded continuously over a period of 3 days.

3.3.2 Porosity

The samples were analysed with a High Throughput Surface Area and Porosity Analyzer, that determines the Brunauer-Emmett-Teller (BET) surface area. The hardened samples were crushed to a fine powder and pre-treated using a SmartPrep instrument to remove adsorbed contaminants from the surface and pore structure. Degassing was first conducted at 60°C but it failed removing the moisture for some samples, so 120°C was also tested. Mild degassing temperatures were used to ensure the preservation of the microstructure of the samples and avoid pore collapse. Nitrogen gas was used as adsorbate due to its inert nature. The technique measures nitrogen adsorption on sample surfaces in order to give specific surface area (m^2/g) and porosity (cm^3/g).

3.3.3 Chemical bonding

To obtain information regarding phase composition and water content, thermogravimetric analysis (TGA) was performed. The hardened samples were crushed into a fine powder and 5–10 mg of each sample was put into small crucibles, then loaded into the instrument. The samples were heated from 35–900°C under a nitrogen atmosphere, with a gas flow of 60 ml/min. The nitrogen gas was used as purge gas due to its inert nature, preventing the samples from oxidizing or combustion. The measurements recorded mass loss as a function of temperature. The data were presented as thermogravimetric (TGA) curves together with derivative thermogravimetric (DTG) curves. Peaks observed in the DTG curves were used to

identify decomposition events and indicate the presence of specific phases within the AAM system.

Fourier Transform Infrared (FTIR) Spectroscopy was used to identify chemical bonds and functional groups present in the samples. The hardened samples were crushed into a fine powder prior to analysis. FTIR measures how much infrared light a sample adsorbs as the wavenumber decreases. The spectra were plotted as transmittance (%) against wavenumber cm^{-1} and the observed peaks corresponds to bending and stretching vibrations of chemical bonds.

3.3.4 Microstructure

Scanning Electron Microscopy (SEM) was used to characterize the microstructure, including surface morphology and phases. Small sections of each sample were embedded in epoxy and ground with sandpaper to obtain a flat and smooth surface for the SEM analysis. Images were created from selected regions of each sample to examine morphological features. Elemental composition was analysed using energy dispersive spectroscopy (EDS), which enabled mapping the distribution of elements within the samples.

3.3.5 Mechanical properties

To evaluate the effect of CPT on the mechanical properties of AAM systems, compressive strength testing was performed. Three different compositions (0% CPT, 20% CPT and 40% CPT) were prepared, with six specimens for each composition. The mixes were produced using sand with a particle size distribution of 0-4 mm as aggregate, at a binder-to-aggregate ratio of 1:3. The materials were mixed using an automated mixer and cast into molds with dimensions of $4 \times 4 \times 4$ cm. Compressive strength was determined using a hydraulic press after curing periods of 7 and 28 days in a climate room at 20°C and 50% relative humidity. The hydraulic press had a maximum load capacity of 15 kN and was operated at a loading rate of 0.500 kN/s. The test was terminated when the applied load decreased to 10% of the maximum load recorded for each sample.

4

Results and discussion

This chapter presents and discusses the experimental results obtained from the characterization of the alkali-activated materials. The results are organized according to reaction kinetics, phase formation, microstructure, and mechanical performance, allowing the influence of CPT incorporation to be evaluated from early-age reactions to final material properties.

4.1 Reaction kinetics and early-age behavior

The early-age behavior of alkali-activated materials is closely linked to the reaction kinetics during dissolution and gel formation. To evaluate the influence of CPT on these processes, setting behavior and heat evolution were investigated using Vicat testing and isothermal calorimetry.

4.1.1 Setting behavior

The initial setting time varied with the CPT ratio in the samples, as can be seen in Figure 4.1. The dropping of the curves corresponds to the hardening of the material. The initial setting time was determined as the point when the Vicat needle penetrates 80% of the sample and is shown in Figure 4.2. Overall, the carbonated samples had faster setting times compared to the non-carbonated ones. The shortest setting time was observed for the sample containing 15% CPT, followed by 10% and 20% CPT. The sample containing 40% CPT is not included in Figure 4.2, as the setting time exceeded 120 minutes, although it eventually hardened.

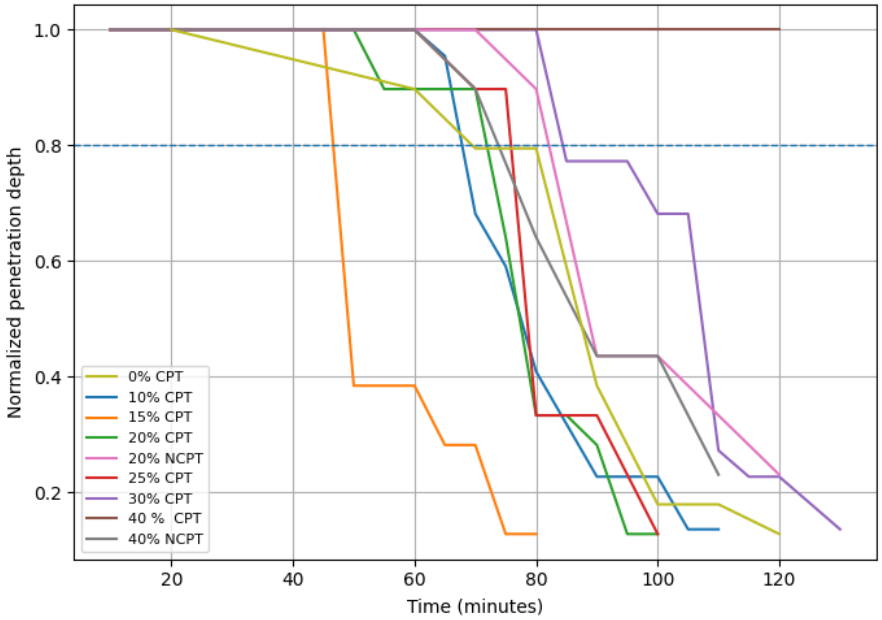

Figure 4.1: Normalized penetration depth as a function of time for samples containing different CPT contents.

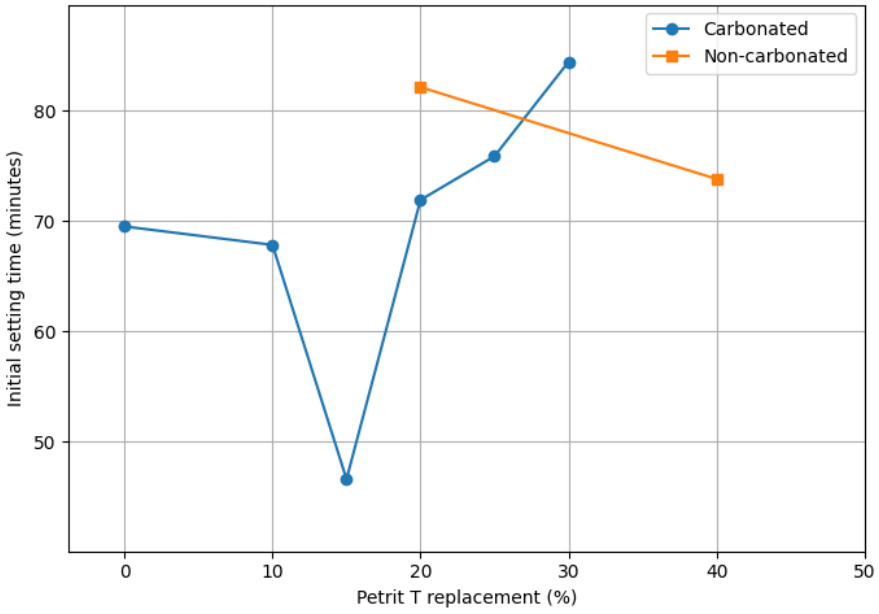

Figure 4.2: Initial setting times for alkali-activated samples containing different replacement levels of CPT and NCPT.

The results suggest that CPT has a non-linear influence on the setting behavior of the material, with the setting time decreasing with increasing CPT content, up to 15% CPT, and then increasing again with higher replacement levels. It should be noted that there is no universally optimal setting time, as the requirements vary depending on the intended application. Nevertheless, materials with initial

setting times between 35 minutes and 6.5 hours are often preferred for construction applications [6]. The 20% CPT sample had a faster setting time than both the 0% CPT and 20% NCPT samples, suggesting that carbonation of the binder influences the reaction kinetics and has a clear influence on the setting behavior of the system.

4.1.2 Heat evolution

The first two exothermic peaks from the isothermal calorimetry data are shown in Figure 4.3, where the local maxima of each peak are marked with a dot. The first peak is strongly exothermic and corresponds to the early dissolution of the precursor and the initial gel formation. The second peak can be attributed to continued gel polymerization, as well as crystallization and stabilization of the hydration products [15]. Figure 4.4 shows that the NCPT sample has a much earlier first peak compared to the other samples, with a relatively small standard deviation. This indicates that the presence of Petrit T accelerates the initial reaction, particularly in its non-carbonated state. However, this observation is not consistent with the results obtained from the Vicat setting measurements. The reason for the inconsistency between the two methods remains unclear and needs further investigation. The samples with 0%, 20% and 40% CPT have similar average times for the first peak, but with noticeably larger standard deviations.

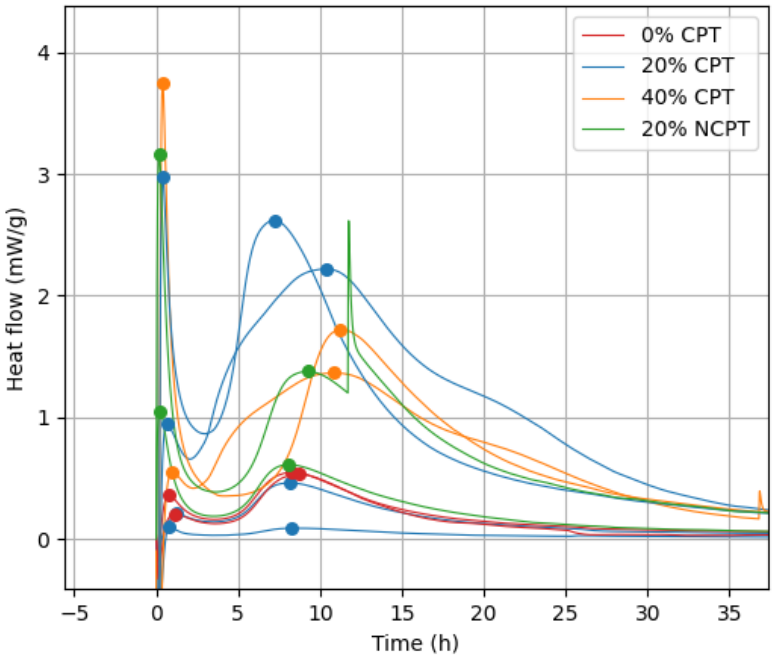

Figure 4.3: Heat flow measured by isothermal calorimetry during the first 35 hours of reaction.

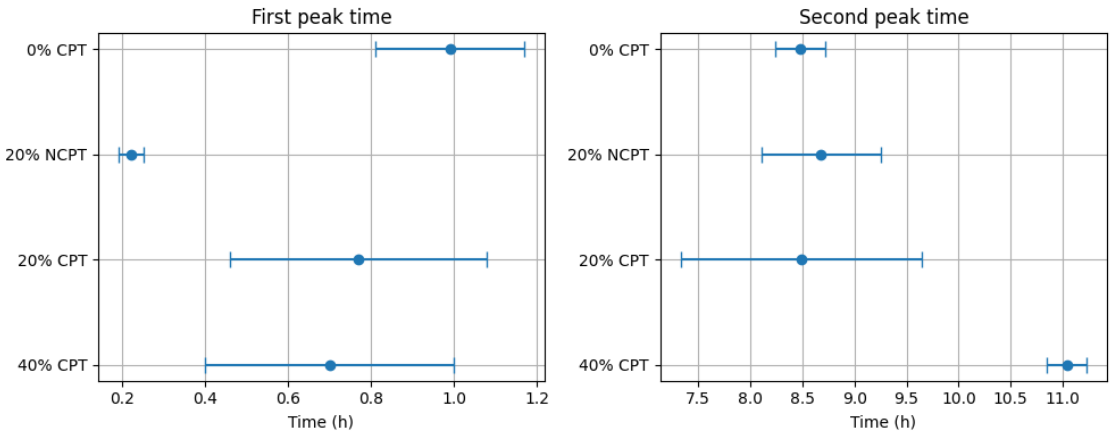

Figure 4.4: Average occurrence time of the first and second calorimetric peaks for the samples, including standard deviation.

The second peak times are also visualized in Figure 4.4. The 40% CPT sample reaches this peak significantly later, at around 11 hours, while the other samples peaks at approximately 8.5 hours. This suggests that increasing the CPT content slows down the later stages of the reaction. Possible reasons include dilution of reactive species, changes in ion availability in the solution, or differences in nucleation conditions. The standard deviation is relatively low for the 0% CPT and 40% CPT samples, but higher for the 20% CPT sample. Since the 20% CPT was tested with four replicates, compared to two for the other samples, the larger spread suggests that this composition is more sensitive to variations in mixing or sample preparation.

Overall, the calorimetry results are not fully consistent between replicates. This is likely due to manual mixing prior to testing, rather than a standardized mixing procedure. While the heat flow per mass varies considerably between samples, the timing of the two main peaks shows clearer and more consistent trends.

4.2 Phase formation

To understand how the incorporation of CPT influences the reaction products, the phase assemblage was investigated using thermogravimetric analysis and FTIR spectroscopy. These techniques provide information regarding gel formation, bound water and the presence of carbonate-containing phases.

4.2.1 Thermogravimetric analysis

Thermogravimetric analysis was performed on five samples and the mass loss as a function of temperature was evaluated. As shown in figure 4.5, the carbonated Petrit T raw material (not alkali-activated) exhibited a more prominent mass loss at higher temperatures compared to the alkali activated samples. This suggests that the raw CPT contained thermally stable carbonate phases, while the alkali-activation of the samples led to less stable reaction products. The samples with 0%

CPT and with 20% NCPT showed similar mass loss curves, indicating that their phase compositions are comparable.

The derivative thermogravimetric (DTG) curves, shown in Figure 4.6, represent the rate of mass change as a function of temperature. This enables the identification of decomposition events that are associated with specific phases. The DTG curves clearly show differences between the alkali-activated samples and the raw CPT material.

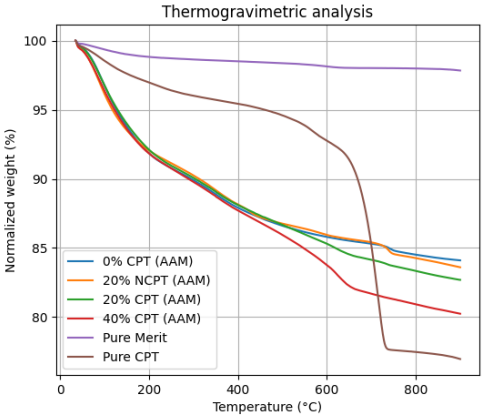

Figure 4.5: TGA curves showing mass loss as a function of temperature for raw CPT, raw Merit and alkali-activated samples.

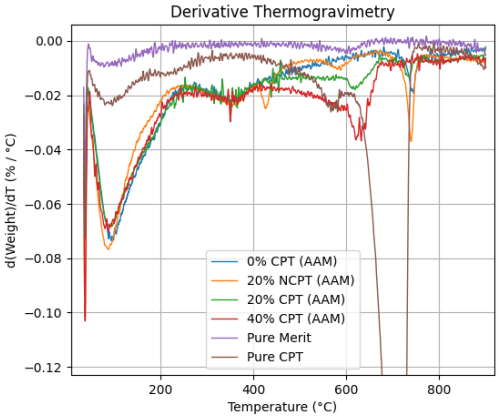

Figure 4.6: DTG curves showing the rate of mass loss as a function of temperature for raw CPT, raw Merit and alkali-activated samples.

The first peak, observed at approximately 40°C corresponds to the loss of free and physically bound water present in the samples. All samples exhibited this peak at similar magnitude in this temperature range, suggesting comparable amounts of water in the samples as well as similar incorporation of water within the structure of the material.

The peak at 90°C corresponds to the dehydration of C–A–S–H gels [5]. This peak was present in all alkali-activated samples but absent in the raw CPT material, confirming successful alkali activation and gel formation. The peak was slightly less pronounced for the samples containing CPT, which may indicate the formation of a smaller amount of binding gel. All alkali-activated samples showed peaks around 350°C, corresponding to decomposition of hydrotalcite phases [5]. Carbonate decomposition peaks were observed in the area between 600 and 800°C [5].

The 20% CPT and 40% CPT show carbonate related peaks at 620°C, while the raw CPT exhibited a larger carbonate peak near 720°C. The carbonate peaks in the 0% CPT and 20% NCPT samples were observed at a higher temperature, around 740°C. All samples except the raw Merit material showed one or more carbonate-related peak, and the intensity of these peaks increased with increasing CPT content. This suggests that there is a higher concentration of carbonate phase in the

alkali-activated samples with higher CPT content. It indicates that the carbonate phases remain present in the sample after alkali-activation and contributes to the decomposition behavior of the material.

4.2.2 FTIR spectroscopy

FTIR analysis, illustrated in Figure 4.7, shows peaks at 3400 and 1700 cm^{-1}, which corresponds to the stretching and bending of O–H bonds. This indicates the presence of absorbed and chemically bound water within the gel structure [15] [17] [18]. Bands observed at approximately 950 and 440 cm^{-1} corresponds to Si–O–T and T–O vibrations, where T represents Si or Al tetrahedron. These bands are characteristic for C–A–S–H gels formed by alkali-activation [15] [17] [18]. The presence of these bonds confirms the gel formation, and their relative consistent positions in the spectra suggests that the overall gel structure is similar independently on CPT content.

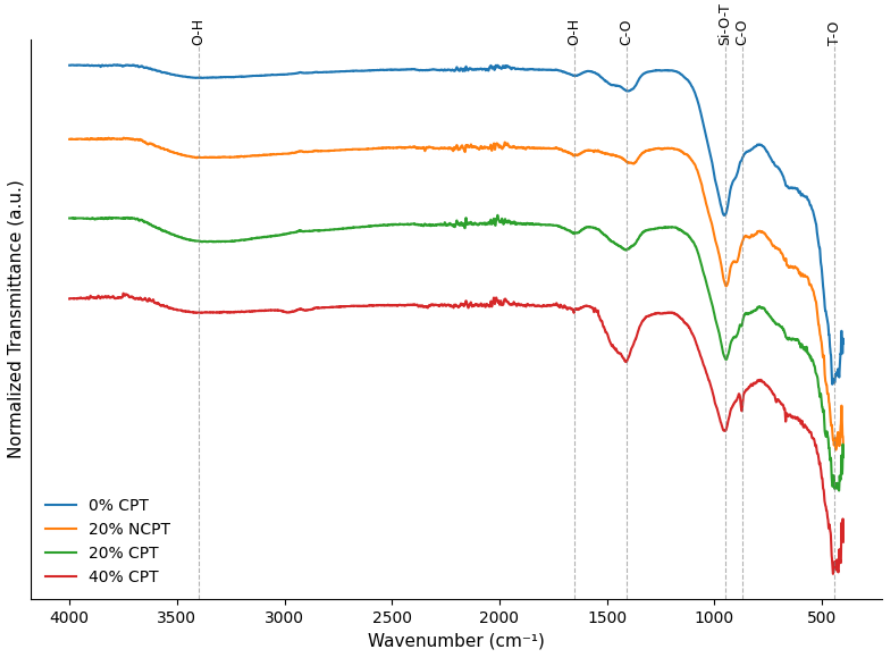

Figure 4.7: Normalized FTIR spectra of alkali-activated samples with varying CPT contents, plotted as transmittance versus wavenumber.

Carbonate related C–O vibrations were identified at approximately 1400 and 870 cm^{-1} [15] [17] [18]. The intensity of these peak increased with increasing CPT content, as the 40% CPT showed the most pronounced carbonate bands. This is due to the larger amount of carbonated material incorporated in the system, and is also aligning with the TGA results, which also showed increased carbonate decomposition with increasing CPT content.

4.3 Microstructure and porosity

The physical structure of the alkali-activated materials was characterized to assess how CPT affects pore development and phase distribution. Porosity measurements and scanning electron microscopy were therefore used to investigate changes in microstructure resulting from CPT incorporation.

4.3.1 Porosity

Both the total pore volume and the BET surface area were higher in the samples containing CPT compared to the 0% CPT sample. Additionally, both parameters increased with increasing CPT content, as shown in Table 4.1, indicating an approximately proportional relationship between CPT content and porosity development.

Table 4.1: Pore characteristics and BET surface area of the investigated samples.

Sample	Total pore volume (cm^3/g)	BET surface area (m^2/g)
Pure CPT	0.093794	43.8677
0% CPT	0.01546	4.0994
20% CPT	0.02146	6.3209
40% CPT	0.03334	9.1954

The pure CPT (not alkali-activated) sample shows significantly higher porosity and surface area than the activated samples. This suggests that CPT contributes to the development of a more porous microstructure in the alkali-activated material. The increased surface area observed with highest CPT content could be attributed to the larger presence of $CaCO_3$, compared to the free, reactive Ca^{2+} ions. This likely reduces the amount of calcium available for the formation of C–A–S–H gel phases, resulting in a less dense and more porous network.

4.3.2 Elemental composition

The morphology of the samples containing 0%, 20%and 40% CPT is presented in Figure 4.8. In image (a), corresponding to 0% CPT, the larger angular features are attributed to unreacted Merit particles that have not participated in gel formation. In images (b) and (c), similar unreacted Merit grains are observed, along with additional unreacted CPT particles. Those granules are amorphous calcium silicate that has not dissolved and XRD results, presented in Appendix A.1, A.2 and A.3, shows noisy signals that have limited evidence of crystalline phases. This indicates that the undissolved particles are primarily amorphous. Therefore, the uncompleted reaction is likely due to insufficient wetting or dissolution of the particles and not because of low solubility caused by crystallinity.

Cracking is evident across all samples and is most likely associated with drying or internal shrinkage during curing and storage.

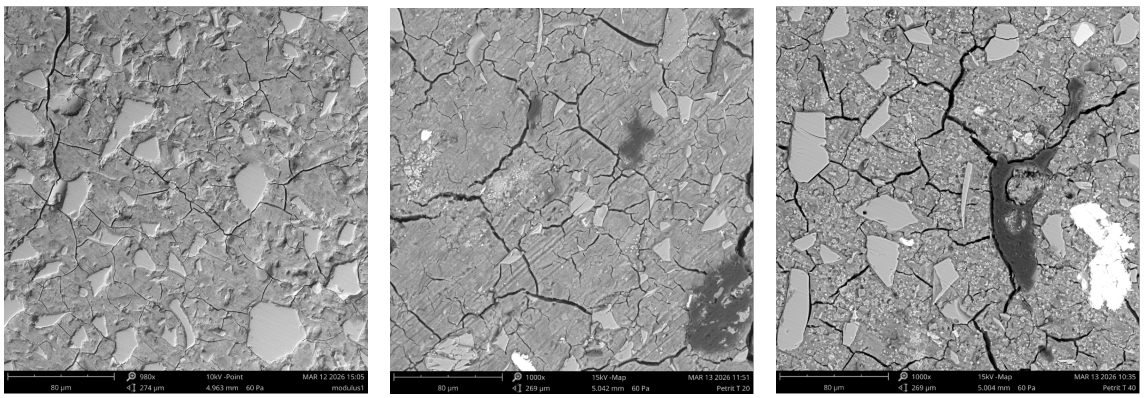

(a) 0% CPT **(b)** 20% CPT **(c)** 40% CPT

Figure 4.8: SEM micrographs of alkali-activated materials containing different CPT replacement levels: (a) 0% CPT, (b) 20% CPT, (c) 40% CPT.

In the sample containing 40% CPT, numerous small bright particles are distributed throughout the matrix. These are identified as calcite [19, 20]. The relatively homogeneous distribution suggests that they originate from the carbonated binder (CPT), with a possible minor contribution from secondary carbonation due to exposure to atmospheric CO_2.

Table 4.2: EDS images showing the presence of four different elements in samples containing 0%, 20% and 40% CPT.

	Calcium	**Aluminum**	**Magnesium**	**Carbon**
0% CPT	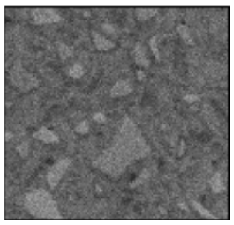	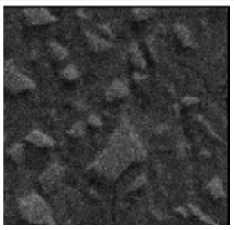	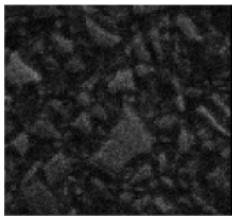	
20% CPT	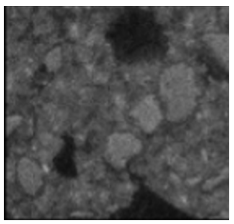	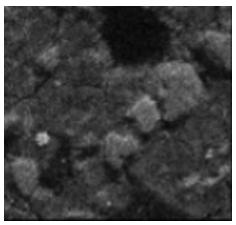	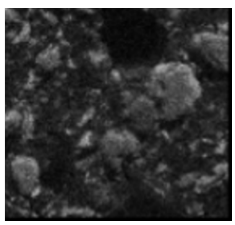	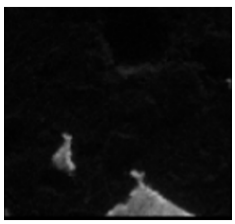
40% CPT	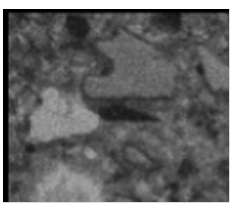	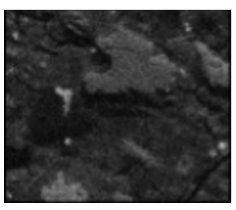	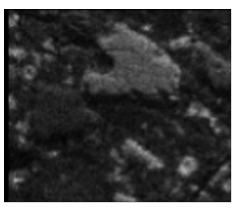	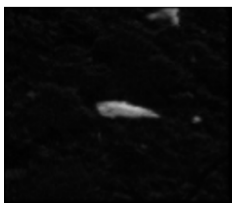

EDS was used to evaluate the spatial distribution of elements, as summarized in Table 4.2. In the 0% CPT sample, calcium is present both within the larger Merit particles and in the surrounding gel phases. Aluminum appears more dispersed throughout the matrix, whereas magnesium remains largely confined to the unreacted Merit, indicating limited dissolution. In contrast, carbon associated with the CPT particles remains localized within the larger grains and shows no significant redistribution into the matrix. This suggests that the carbon particles, and likely the iron particles seen in Fig 4.8, behaves more as inert fillers than reactive binders.

4.4 Mechanical performance

The performance of alkali-activated materials is strongly influenced by their reaction products and microstructure. To evaluate the practical consequences of CPT incorporation, compressive strength measurements were performed and connected to the observed porosity and phase development.

4.4.1 Compressive strength

The incorporation of CPT significantly reduced the compressive strength, as shown in Figure 4.9. This indicates that CPT does not contribute positively to strength developing of the samples and may instead disrupt the binder matrix. The relatively low standard deviations indicates that the observed trends are systematic rather than random experimental variation.

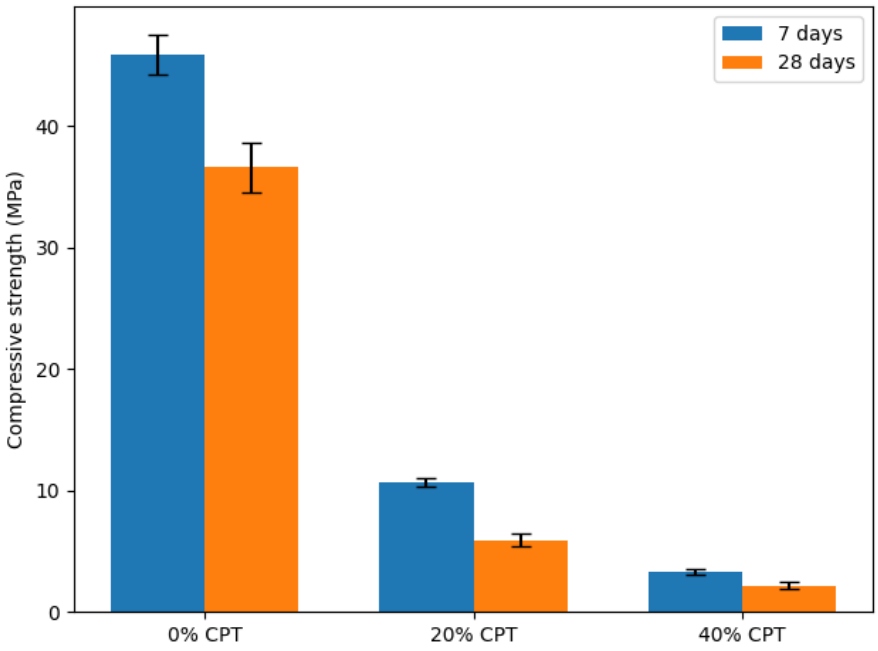

Figure 4.9: Compressive strength of alkali-activated samples containing different CPT contents after 7 and 28 days of curing.

One possible contributor to the reduced strength is the increased porosity observed

in the BET analysis. Both the total pore volume and specific surface area increased with increasing CPT content, indicating the formation of a less dense microstructure. Higher porosity reduces load-bearing capacity and increases crack formation, which both results in lower the compressive strength.

In addition, the carbonation of the slag beforehand reduced reactive calcium species to stable carbonate phases like $CaCO_3$, which might lead to less formation of C–A–S–H gel phases. A lack of gel network formation or a less continuous matrix will have a negative effect on the strength development in the AAM and will thus become mechanically weaker. The SEM observation support this interpretation, as unreacted CPT particles are seen within the matrix, indicating a limited participation in the alkali-activating reaction. It could mean that the CPT acts more as an inert filler than a reactive binder precursor, especially at higher replacement levels.

All compositions showed lower compressive strength after 28 days compared to 7 days. This behavior is not normal for alkali-activated materials and may be related to drying shrinkage or microcracking during curing. Another possible explanation is the curing conditions, which could have led to moisture loss and hindered further gel development, or an insufficient water-to-binder ratio. Another possible explanation for the unexpectedly higher compressive strength of the 7-day samples is related to differences in sample preparation. The 7-day cured samples were prepared after the 28-day samples, and experience gained during the preparation of the latter may have led to improvements in the mixing procedure. Thus, the 7-day samples may have been mixed more effectively, resulting in more homogeneous mixtures and reduced air entrapment. Further investigations are required to determine the cause of the strength reduction.

5
Conclusion

This thesis investigated the use of carbonated Petrit T (CPT) as a co-binder in alkali-activated materials. The influence of CPT on reaction kinetics, phase formation, microstructure, porosity and mechanical performance was investigated using different characterization techniques.

The results showed that CPT has a significant influence on the reaction mechanisms of the alkali-activated systems. Low replacement levels of CPT seemed to speed up the initial setting behavior, while high replacement levels speed up the later stages of the reaction. This indicates that CPT has a non-linear effect on the reaction kinetics, and may initially promote gel formation, but reduce the overall reactivity of the system at higher replacement levels.

TGA and FTIR analyses confirmed the formation of C–A–S–H gel phases in all alkali-activated samples, supporting that the activation of the binders was successful. Increasing CPT content also showed more pronounced carbonate-related phases, indicating that the carbonates introduced to the CPT remained present after alkali-activation. SEM and EDS analyses showed the presence of unreacted CPT particles throughout the matrix, indicating that they behaved more as a filler than participating in gel formation.

BET analysis showed that increasing CPT content increased both the pore volume and the specific surface area of the materials, signaling the formation of a more porous microstructure. This aligned with the compressive strength measurements, where increasing CPT content significantly reduced the mechanical strength. The reduced strength could be related to lower availability of reactive calcium species for C–A–S–H formation, which then results in a less dense and weaker gel network.

The results indicate that the carbonated steel slag can be incorporated into alkali-activated materials and contributes to CO_2 utilization through carbonation. However, at the investigated replacement levels, CPT had a negative effect on the mechanical performances of the material. It is suggested that optimization of parameters such as activator composition, curing conditions and replacement levels is necessary to improve the material performance.

5.1 Future work

Further work should focus on optimizing the alkali-activator composition, analysing long-term durability and evaluating whether lower CPT replacement levels or different curing conditions can improve the mechanical properties of the system.

5.2 Disclosure and declaration of AI use

AI-tools was used during this thesis as a support for data processing, coding assistance and for language and grammar improvements.

Bibliography

[1] Siyao Guo et al. “Sodium-based activators in alkali- activated materials: Classification and comparison”. In: *Journal of Building Engineering* 70 (July 2023), p. 106397. ISSN: 2352-7102. DOI: 10.1016/J.JOBE.2023.106397.

[2] Ming Ren et al. “Negative emission technology is key to decarbonizing China’s cement industry”. In: *Applied Energy* 329 (Jan. 2023), p. 120254. ISSN: 0306-2619. DOI: 10.1016/J.APENERGY.2022.120254.

[3] P. E. Tsakiridis et al. “Utilization of steel slag for Portland cement clinker production”. In: *Journal of Hazardous Materials* 152.2 (Apr. 2008), pp. 805–811. ISSN: 0304-3894. DOI: 10.1016/J.JHAZMAT.2007.07.093.

[4] Markssuel Teixeira Marvila, Afonso Rangel Garcez de Azevedo, and Carlos Maurício Fontes Vieira. “Reaction mechanisms of alkali-activated materials”. In: *Revista IBRACON de Estruturas e Materiais* 14.3 (2021). ISSN: 19834195. DOI: 10.1590/S1983-41952021000300009.

[5] S. U. Bo et al. “Carbonated steel slag as a dual-function additive for strength and sustainability enhancement of alkali-activated slag”. In: *Process Safety and Environmental Protection* 203 (Nov. 2025), p. 107868. ISSN: 0957-5820. DOI: 10.1016/J.PSEP.2025.107868.

[6] Haimei Zhang. *Cement*. Woodhead Publishing, Jan. 2011, pp. 46–423. DOI: 10.1533/9781845699567.46.

[7] John Provis and Jannie Deventer. *Alkali Activated Materials*. Vol. 13. Dordrecht: Springer Netherlands, 2014. ISBN: 978-94-007-7671-5. DOI: 10.1007/978-94-007-7672-2.

[8] Ismail Amer et al. “A review on alkali-activated slag concrete”. In: *Ain Shams Engineering Journal* 12.2 (June 2021), pp. 1475–1499. ISSN: 20904479. DOI: 10.1016/j.asej.2020.12.003.

[9] A. Buchwald and M. Schulz. “Alkali-activated binders by use of industrial by-products”. In: *Cement and Concrete Research* 35.5 (May 2005), pp. 968–973. ISSN: 00088846. DOI: 10.1016/j.cemconres.2004.06.019.

[10] F. Puertas et al. “A model for the C-A-S-H gel formed in alkali-activated slag cements”. In: *Journal of the European Ceramic Society* 31.12 (Oct. 2011), pp. 2043–2056. ISSN: 0955-2219. DOI: 10.1016/J.JEURCERAMSOC.2011.04.036.

[11] Qiu Li, Andrew P. Hurt, and Nichola J. Coleman. "The application of 29Si NMR spectroscopy to the analysis of calcium silicate-based cement using Biodentine™ as an example". In: *Journal of Functional Biomaterials* 10.2 (2019). ISSN: 20794983. DOI: 10.3390/JFB10020025.

[12] Jiazhi Huang and Baomin Wang. "Non-classical nucleation mechanisms of C-A-S-H gel in alkali-activated slag: A multi-scale modeling and experimental investigation". In: *Chemical Engineering Journal* 525 (Dec. 2025), p. 169347. ISSN: 1385-8947. DOI: 10.1016/J.CEJ.2025.169347.

[13] Alireza Kashani et al. "Carbon utilization for low-carbon concrete: Prospects for carbonated steel slag and recycled concrete". In: *Resources, Conservation and Recycling* 226 (Feb. 2026), p. 108698. ISSN: 0921-3449. DOI: 10.1016/J.RESCONREC.2025.108698.

[14] Qifeng Song et al. "Contribution of calcium-containing minerals on the mechanical properties of alkali-activated materials: A study of carbonation steel slag". In: *Construction and Building Materials* 468 (Mar. 2025), p. 140451. ISSN: 18790658. DOI: 10.1016/j.resconrec.2021.105740.

[15] Yang Liu et al. "Ultra-early strength and carbon benefits alkali-activated materials based on carbonation steel slag". In: *Process Safety and Environmental Protection* 208 (Mar. 2026), p. 108516. ISSN: 0957-5820. DOI: 10.1016/J.PSEP.2026.108516.

[16] Emmanouela Leventaki et al. "Aqueous mineral carbonation of three different industrial steel slags: Absorption capacities and product characterization". In: *Environmental Research* 252.4 (July 2024), p. 118903. ISSN: 10960953. DOI: 10.1016/j.envres.2024.118903.

[17] Yang Liu et al. "Contribution of calcium-containing minerals on the mechanical properties of alkali-activated materials: A study of carbonation steel slag". In: *Construction and Building Materials* 468 (Mar. 2025), p. 140451. ISSN: 0950-0618. DOI: 10.1016/J.CONBUILDMAT.2025.140451.

[18] Zengqing Sun et al. "Steel slag for carbon fixation and synthesis of alkali-activated material". In: *Construction and Building Materials* 351 (Oct. 2022), p. 128959. ISSN: 0950-0618. DOI: 10.1016/J.CONBUILDMAT.2022.128959.

[19] Anbuthangam Ashokan, T. S.Sampath Kumar, and Guhan Jayaraman. "Process optimization for the rapid conversion of calcite into hydroxyapatite microspheres for chromatographic applications". In: *Scientific Reports 2022 12:1* 12.1 (July 2022), pp. 12164–. ISSN: 2045-2322. DOI: 10.1038/s41598-022-16579-4.

[20] Damir Kralj et al. "Effect of Inorganic Anions on the Morphology and Structure of Magnesium Calcite". In: *Chemistry - A European Journal* 10.7 (Apr. 2004), pp. 1647–1656. ISSN: 09476539. DOI: 10.1002/CHEM.200305313;WGROUP:STRING:PUBLICATION.

A

Appendix

A.1 XRD diffractograms

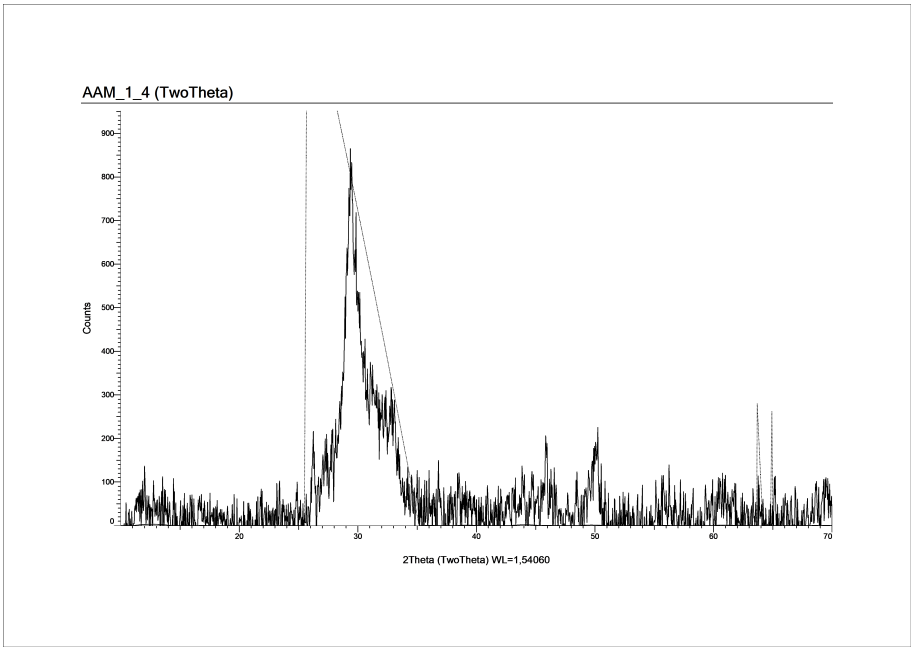

Figure A.1: XRD results for sample containing 0% CPT

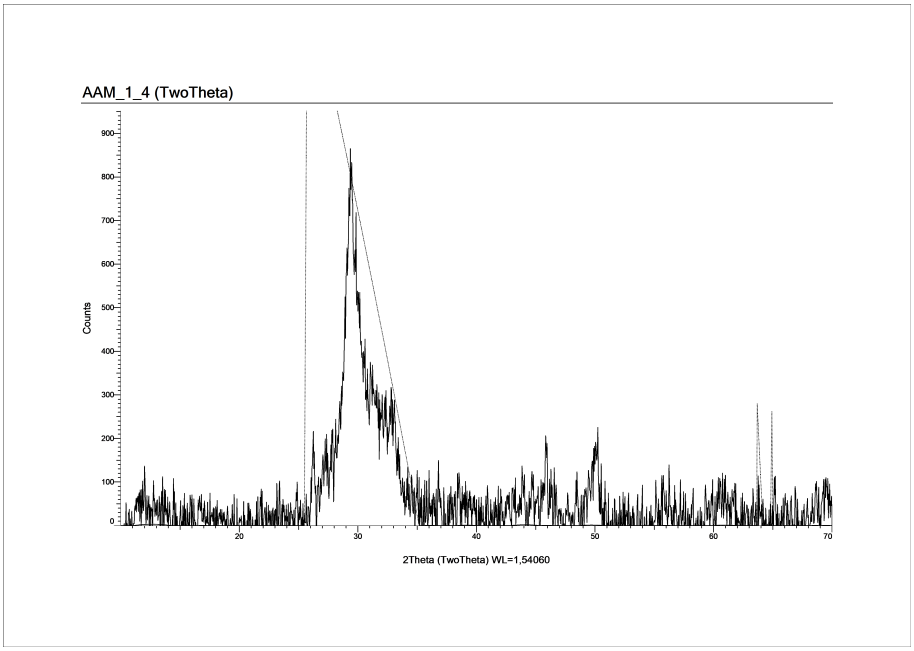

Figure A.2: XRD results for sample containing 20% CPT

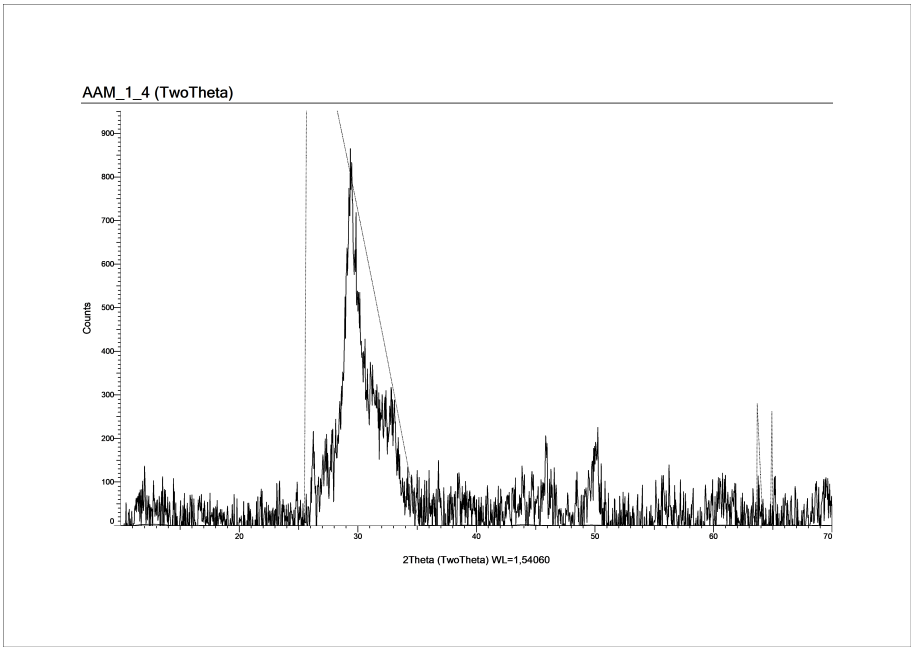

Figure A.3: XRD results for sample containing 20% NCPT

DEPARTMENT OF SOME SUBJECT OR TECHNOLOGY
CHALMERS UNIVERSITY OF TECHNOLOGY
Gothenburg, Sweden
www.chalmers.se

CHALMERS
UNIVERSITY OF TECHNOLOGY